Global Journal of Environmental Science and Technology: ISSN-2360-7955
Abbreviated Key Title: Glob. J. Environ. Sci. Technol. ISSN: Open Access.
Vol. 13(4): Pp. 19-38, May, 2026. https://doi.org/10.54978/gest/2025

OPEN ACCESS

Full Length Research

Efficient Removal of Chromium from Real Tannery Wastewater Using Modified Cordia africana Sawdust

[1]Gebrearegaya, A. W., [2]Tesfaye, M., & [3]Gizaw, A.

[1]PhD candidate in Adama Science and Technology University in Chemical Engineering Department , Adama , Ethiopia. hubadama@gmail.com
[2]Associate profesor in Adama Science and Technology University in Chemical Engineering Department , Adama , Ethiopia.
[3]Assistant profesor Adama Science and Technology University in Chemical Engineering Department , Adama , Ethiopia
Corresponding author: Aster Woldu , hubadama@gmail.com, +251 0912 154243

Abstract

Chromium pollution from tannery wastewater is a major concern for the environment and public health, especially for developing nations wherein the available treatment technologies do not prove effective and are expensive. Hexavalent chromium (Cr^{6+}) is known for its toxic nature and high mobility and stability in water bodies. Notably, the identification and development of low-cost and efficient adsorbents for chromium pollution abatement in tannery wastewater is a pressing requirement. Cordia africana sawdust was utilised to develop adsorbent materials, namely raw sawdust (SD), acid functionalised sawdust (AMSD), and iron nanoparticle-loaded polyvinyl alcohol-coated sawdust (FeNP-SD-PVA). The real tannery wastewater, collected from Batu Tannery in Ethiopia, underwent pretreatment followed by characterisation for physicochemical parameters and chromium species. Adsorption experiments using a batch method were done to determine chromium removal capacity. Additionally, interference experiments, which involved selectively excluding dominant co-constituent ions as well as organic components, were done to determine their chromium adsorption effect. All experiments were performed in triplicate. Removal efficiencies of highest values of 90.29% ± 1.24% for Cr^{6+}, 81.67% ± 1.08% for Cr^{3+}, and 83% ± 1.15% for total chromium were shown by the FeNP-SD-PVA composite. Moderate effectiveness of AMSD and poor adsorbing capacity of raw sawdust were observed with lower sensitivities towards interference ions. Robust resistances towards interference ions and high efficiencies were found in the case of the FeNP-based adsorbent. Statistical analysis (one-way ANOVA) confirmed significant differences among adsorbents ($p < 0.05$). The outcomes of this study show the effectiveness of iron nanoparticle-modified Cordia africana sawdust for the removal of chromium from tannery wastewater. This method has shown promise for being a feasible option for the treatment of tannery wastewater.

Keywords: Chromium, Wastewater, Adsorption, Nanoparticles, Public Health

Accepted: 6/4/2026 Published: 1/5/.2026

1. Introduction

Chromium exists in several oxidation states, each with different chemical behaviours and biological impacts. The most stable and least toxic trivalent chromium (Cr^{3+}) is recognised to participate in carbohydrate metabolism in humans, but hexavalent chromium (Cr^{6+}) is highly soluble and mobile and up to one hundred times more toxic than Cr^{3+} due to its strong oxidising property, enhancing the formation of reactive intermediates capable of cellular and genetic damage (El Moussaoui O, et al., 2023). Cr^{6+} does not occur in free form in nature; instead, it is generated mainly by industrial activities like chrome plating, textiles, pigment manufacturing, and leather tanning. Chromium sulphate is used in large proportions in chrome tanning to change raw hides into leather, while in practice, about 40% of the applied chromium does not bind to the hide and is discharged along with wastewater, causing environmental contamination (Berehanu B et al., 2020). Ethiopia is home to over 27 operational tanneries, with the majority using chrome-based tanning methods due to their speed, economy, and high-quality leather production. However, chrome tanning produces massive amounts of wastewater characterised by high levels of chromium; organic matter in the forms of COD and BOD; suspended solids; sulphides; chlorides; and other dissolved

pollutants, as indicated in Figure 1 (Berehanu B et al., 2020). Various Ethiopian tannery wastewater studies have recorded chromium levels well above the recommended limits. In some facilities, the levels of total chromium in untreated wastewater have reached up to about 26 mg/L (Bayesa H, et al., 2015). Waste discharged from tanning industries into rivers such as the Little Akaki River has caused perpetual pollution, where even after treatment, chromium, sulphide, and other parameters have remained above the permissible levels for discharge. Wastewater from the Sheba Leather Industry in northern Ethiopia has been proven to accumulate chromium in vegetables that are irrigated using contaminated water, thus showing that heavy metals could be transferred to the food chain (APHA, 2017).

The complexity of tannery wastewater, combined with the fact that conventional treatment systems have proved inadequate, especially in low-income countries, demands effective low-cost methods for chromium removal. Though there are various technologies currently available, such as ion exchange, membrane filtration, chemical precipitation, and electrochemical processes, most of them are prohibitively expensive, produce secondary waste, or require technical expertise. As a result, adsorption has emerged as a practical and efficient alternative for removing heavy metals from wastewater because of its simplicity, low operational cost, and adaptability. At particular appeal are low-cost adsorbents derived from natural materials and industrial or agricultural wastes because they are abundant, inexpensive and require minimal processing.

While numerous studies have explored agricultural wastes like rice husk, banana peel, or other sawdust types for heavy metal adsorption, the specific use of Cordia africana sawdust, particularly in its raw, acid-modified, and iron nanoparticle-polyvinyl alcohol composite forms applied to real tannery wastewater from an Ethiopian facility, represents a novel application. Furthermore, detailed interference studies by selectively suppressing co-existing ions to evaluate their impact on chromium adsorption add methodological originality, as such targeted suppression experiments are less common in similar biosorbent studies.

In this work, Cordia africana sawdust was utilised as a base material for the preparation of low-cost adsorbents for chromium removal from real tannery wastewater. Hence, the sawdust was processed into raw and acid-modified forms, and a composite material loaded with iron nanoparticles (FeNP-SD-PVA) was synthesised to increase the adsorption performance. Real tannery wastewater was collected, pretreated and characterised for pH, electrical conductivity, total dissolved and suspended solids, COD, total chromium, Cr^{6+}, Cr^{3+}, sulphate, chloride, hardness and competing metal ions by following established methods (Politi M & Sidiras D, 2020). Further, interference studies were conducted by selectively suppressing ions like sulphate, chloride, calcium, magnesium, iron, copper and zinc in order to see their influence on chromium adsorption. Then, batch adsorption tests were conducted to see the efficiency of the prepared adsorbents. This approach provides a comprehensive assessment of chromium and nutrient removal from tannery wastewater using low-cost, locally available materials.

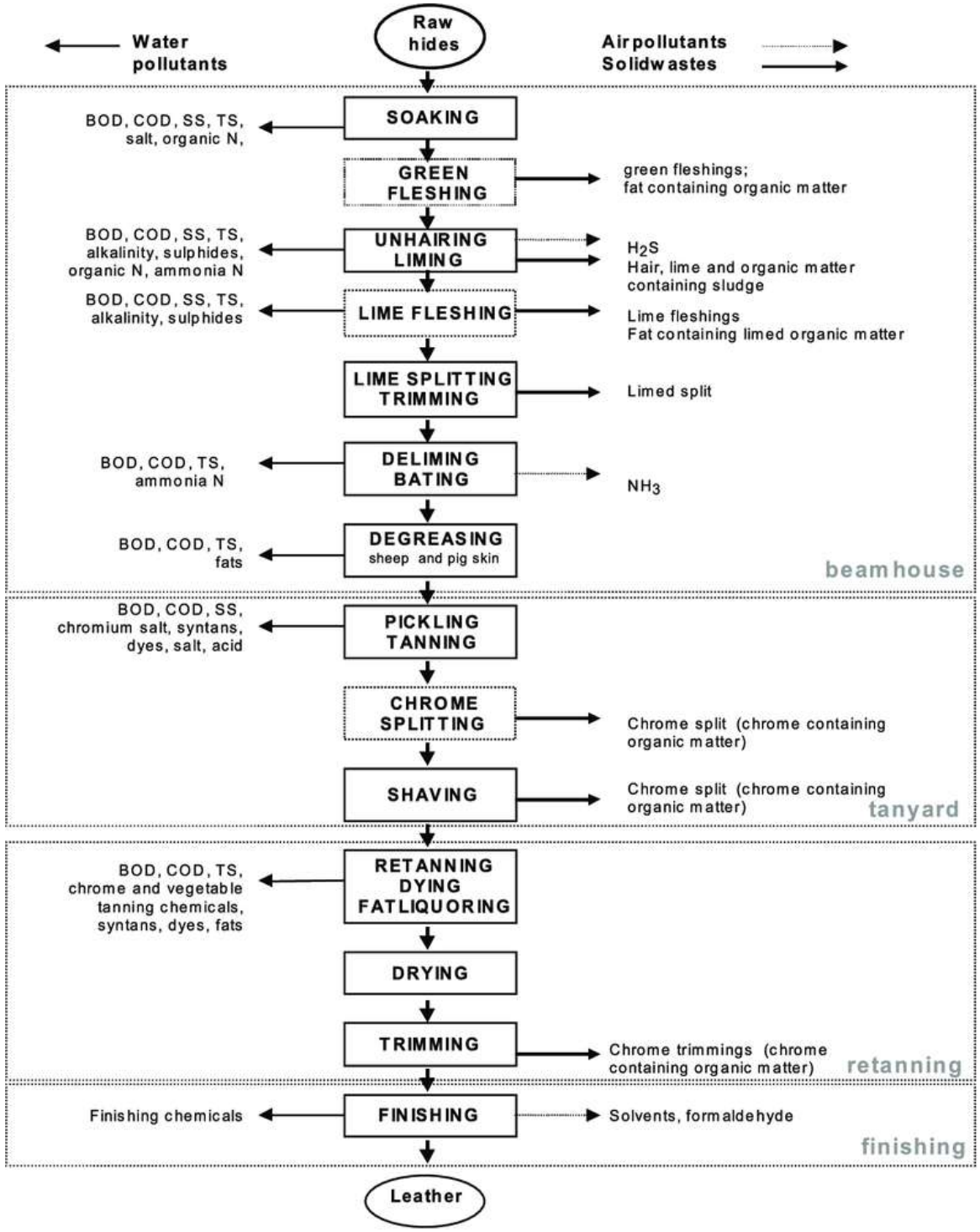

Figure 1. Flow diagram for leather processing

2. MATERIALS AND METHODS

2.1 Chemicals and Reagents

All chemicals used were of analytical grade and used without further purification. Iron(II) sulphate heptahydrate ($FeSO_4 \cdot 7H_2O$, 99%) was sourced from Lab Tech Import Trading (Ethiopia). Polyvinyl alcohol (PVA; MW ≈ 30,000–70,000) was purchased from Sigma-Aldrich. Potassium dichromate ($K_2Cr_2O_7$, 99.8%) served as the Cr(VI) source.

H_2SO_4 was used to produce acid-modified adsorbent. Hydrochloric acid (HCl, 37%) and sodium hydroxide (NaOH, 98%) were used to adjust pH. To study interference effects, these chemicals were also used: $BaCl_2$ solution (0.1 M), $AgNO_3$ solution (0.1 M), Na_2CO_3 solution (0.1 M), NaOH solution (0.1 M) and activated carbon.

2.2 Preparation of Raw Sawdust

Sawdust Collection and Pre-treatment:

Raw sawdust (R-SD) was collected from *Cordia africana* wood waste at Abera Wanza Wood Sales (Addis Ababa, Ethiopia). The material was sun-dried, sieved to a particle size of 250–500 µm, thoroughly washed with distilled water, and oven-dried at 105 °C for 24 hours **(**Aragaw TA & Bogale FM, 2023**).**

2.3 Sawdust modification with acid

Ten grams of dried sawdust were mixed with 100 mL of 1:1 v/v H_2SO_4 : H_2O, stirred for 60 min at 25 °C, filtered, rinsed to neutral pH and re-dried (105 °C, 24 h). The product is referred to as acid-modified sawdust (AM-SD) (Deng X et al., 2024).

2.4 Synthesis of FeNP-SD-PVA Composite

Step 1 – Iron Nanoparticles (FeNPs) Preparation:

$FeSO_4 \cdot 7H_2O$ (0.5 g) was dissolved in 50 mL of distilled water and stirred at 700 rpm. NaOH (0.5 g) was added dropwise to reach pH 10–11. After 30 minutes, nanoparticles were collected via centrifugation at 3,500 rpm for 10 minutes and washed three times with distilled water.

Step 2 – Composite Formation:

Five grams of pretreated sawdust were mixed with the freshly prepared FeNPs in 50 mL of 1% PVA solution and stirred for 2 hours at room temperature. The mixture was vacuum-filtered, then oven-dried at 105 °C for 24 hours. The final FeNP-SD-PVA composite was stored in airtight containers (Bayisa L et al., 2021).

2.5 Preparation of Samples for Interference Studies

As **outlined** in Table 1, to systematically examine the effects of competing ions on chromium adsorption, raw wastewater was divided into eight equal portions (200 mL each) and **put through** selective ion suppression treatments. Each treatment was **planned** to remove or suppress specific interfering ions while preserving chromium species (Cr^{6+} and Cr^{3+}) concentrations.

Table 1: Summary of Ion Suppression Treatments for Interference Studies

Sample Code	Ion Suppressed	Suppression Method	Chemical Used	Target pH	Mechanism
A (Control)	None	No treatment	-	Original	-
B	SO_4^{2-}	Precipitation as $BaSO_4$	10 mL 0.1 M $BaCl_2$	Original	Precipitation
C	Cl^-	Precipitation as AgCl	10 mL 0.1 M $AgNO_3$	Original	Precipitation
D	Ca^{2+}, Mg^{2+}	Precipitation as $CaCO_3$, $Mg(OH)_2$	5 mL 0.1 M Na_2CO_3 + NaOH to pH 10	10.0	Chemical softening
E	Organic matter	Oxidation + Adsorption	5 mL 30% H_2O_2 + 2 g activated carbon	Original	Oxidation/Adsorption
F	Fe^{2+}/Fe^{3+}	Oxidation + Precipitation	Air bubbling + NaOH to pH 7.5–8	7.5–8.0	Oxidation/Precipitation
G	Cu^{2+}	Precipitation as $Cu(OH)_2$	0.1 M NaOH to pH 8.5–9	8.5–9.0	Precipitation
H	Zn^{2+}	Precipitation as $Zn(OH)_2$	0.1 M NaOH to pH 9.5–10	9.5–10.0	Precipitation

For each suppression treatment, the following general procedure was followed: the precipitating agent was added slowly with continuous stirring; the mixture was stirred for 30 minutes (or as specified) to ensure complete reaction; the precipitate was allowed to settle; the supernatant was filtered through Whatman No. 42 filter paper; and pH was recorded before and after treatment. All treated samples were analyzed for chromium concentrations to verify that no chromium loss occurred during suppression procedures.

2.6 Wastewater Characterization

Physicochemical parameters of raw and treated wastewater were analyzed following standard methods (Suryanto F, et al., 2024). All analyses were performed in triplicate, and results were reported as mean ± standard deviation.

Physical Parameters: pH was measured using a calibrated pH meter (Hanna Instruments, HI 2211). Temperature was recorded at the time of collection and during experiments. Electrical conductivity (EC) was determined using a conductivity meter (Hanna Instruments, HI 9835). Total suspended solids (TSS) and total dissolved solids (TDS) were analyzed gravimetrically according to Standard Methods 2540D and 2540C, respectively (Suryanto F, et al., 2024).

Chemical Parameters: Chemical oxygen demand (COD) was determined by the closed reflux colorimetric method (Standard Method 5220D) (Suryanto F, et al., 2024). Hexavalent chromium (Cr^{6+}) was quantified by the 1,5-diphenylcarbazide method using a UV-Vis spectrophotometer (Shimadzu UV-1800) at 540 nm (Loehr RC, 1967). Total chromium was analyzed by atomic absorption spectroscopy (AAS; PerkinElmer AAnalyst 400). Trivalent chromium (Cr^{3+}) concentration was calculated as the difference between total chromium and Cr^{6+}. Sulfate (SO_4^{2-}) was determined by the turbidimetric method (Standard Method 4500-SO_4^{2-}) (Suryanto F, et al., 2024). Chloride (Cl^-) was analyzed by the argentometric method (Standard Method 4500-Cl^- B) (Suryanto F, et al., 2024). Metal ions (Fe, Cu, Zn, Mn, Cd, Ca, Mg) were analyzed by AAS with appropriate hollow cathode lamps and calibration standards.

2.7 Characterizationsof adsorbents

The physicochemical properties of the sample were characterized using several techniques. Fourier-transform infrared (FT-IR) spectroscopy (Nicolet iS50) was performed in the range of 4000–400 cm^{-1} with a resolution of 4 cm^{-1} to identify functional groups. The surface morphology was examined by scanning electron microscopy (SEM) using a JEOL JCM 6000Plus instrument operating at 15 kV. The specific surface area was determined from N_2 adsorption isotherms at 77 K using the Brunauer-Emmett-Teller (BET) method (Horiba SA 9600), following sample degassing at 105 °C for 6 h. The crystallinity was evaluated by X-ray diffraction (XRD) on a Shimadzu XRD 7000 diffractometer with Cu Kα radiation, scanning from 10° to 55° (2θ) at a rate of 2° min^{-1}. Finally, the PZC of the adsorbent was determined using the pH-drift method by equilibrating 0.2 g of adsorbent with 40 mL of 0.1 M $NaNO_3$ solution over an initial pH range of 2–10 for 24 h, and identifying the pH at which ΔpH = 0.

2.8 Batch Adsorption Experiments

To assess the chromium removal efficiency of each adsorbent, batch adsorption experiments were performed. All experiments were done in triplicate, and mean values with standard deviations are reported.

For each adsorption test, 50 mL of wastewater sample (raw or ion-suppressed) was pour in a 250 mL Erlenmeyer flask. Adsorbent (1.0 g) was added, and the mixture was agitated on an orbital shaker at 150 rpm for 2 hours at ambient temperature (25°C ± 2°C). The contact time of 2 hours was selected based on preliminary kinetic studies showing that equilibrium was approached within this period, consistent with literature reports for similar biosorbent systems (Webster T, et al., 2024).

After agitation, samples were filtered through Whatman No. 42 filter paper. The filtrate was analyzed for residual Cr^{6+}, total Cr, competing ions, and COD using the methods described in Section 2.4. Removal efficiency (%) was calculated using the equation:

$$\text{Removal efficiency (\%)} = \left[\frac{(C_o - C_e)}{C_o}\right] X\ 100 \quad (1)$$

where C_0 is the initial concentration (mg/L) and C_e is the equilibrium concentration (mg/L).

2.9 Adsorption Kinetics

Adsorption kinetics of Cr(VI) onto adsorbents were investigated under optimized conditions (pH 3.0 for AMSD, pH 5.5 for raw sawdust andFeNP-SD-PVA Composite, initial concentration 47 mg L^{-1}, adsorbent dose 1 g per 50 mL, and 25 °C). The experimental data were analyzed using nonlinear pseudo-first-order (PFO) and pseudo-second-order (PSO) kinetic models to describe the adsorption rate and mechanism. The nonlinear versions of PFO and PSO models are provided in the equation below.

$$q_t = q_e\left(1 - e^{\frac{-k_1}{t}}\right) \quad \textbf{(3)}$$

$$q_t = \frac{q_e^2 K_2 t}{1 + q_e K_2 t} \quad \textbf{(4)}$$

Where: q_e is adsorption Capacity (mg/g), $K_1(min^-)$ and K_2 (g mg^{-1} min^{-1}) are rate constant and t is time in min.

2.10 Adsorption Isotherms

Equilibrium adsorption experiments were conducted at 25 °C and pH 3.0 for AMSD, pH 5.5 for raw sawdust and FeNP-SD-PVA Composite; using initial Cr(VI)

concentrations ranging from 20 to 50 mg L^{-1}. The equilibrium data were fitted to the Langmuir and Freundlich isotherm models to evaluate adsorption capacity and surface characteristics. Langmuir and Freundlich nonlinear equations are given below.

$$q_e = \frac{q_{max} K_a C_e}{1 + K_a C_e} \quad \textbf{(5)}$$

$$q_e = K_f C^{\frac{1}{n}} \quad \textbf{(6)}$$

Where: q_e is the adsorption capacity at equilibrium (mg g^{-1}), qmax is the maximum monolayer adsorption capacity (mg g^{-1}), K_L is the Langmuir adsorption constant related to affinity of binding sites (L mg^{-1}), Ce is the equilibrium concentration of Cr(VI) in solution (mg L^{-1}). K_F is the Freundlich constant indicative of adsorption capacity (mg g^{-1})(L mg^{-1}), 1/n (mg g^{-1}), n is the Freundlich intensity parameter (dimensionless), and C_e is the equilibrium concentration of Cr(VI) in solution (mg L^{-1}).

2.11 Thermodynamic Studies

Thermodynamic parameters, including Gibbs free energy change (ΔG°), enthalpy change (ΔH°), and entropy change (ΔS°), were determined from temperature-dependent adsorption experiments conducted between 25 and 50 °C. The following equations were used to calculate the standard enthalpy (Δ*H*°), the standard entropy (Δ*S*°), and the Gibbs free energy change (Δ*G*°) for the Cr adsorption on the AM-SD adsorbet .

$$lnK_d = -\frac{\Delta H^\circ}{RT} + \frac{\Delta S^\circ}{R} \quad \textbf{(7)}$$

$$K_d = \frac{q_e}{C_e} \quad \textbf{(8)}$$

$$\Delta G^\circ = \Delta H^\circ + T\Delta S^\circ \quad \textbf{(9)}$$

Where: ΔH° is the standard enthalpy change (kJ mol^{-1}), ΔG° is the standard Gibbs free energy change (kJ mol^{-1}), and ΔS° is the standard entropy change (J mol^{-1} K^{-1}). C_e is the equilibrium concentration of Cr(VI) in solution (mg L^{-1}), q_e is the adsorption capacity at equilibrium (mg g^{-1}), R is the universal gas constant (8.314 J mol^{-1} K^{-1}), T is the absolute temperature (K), and Kd is the distribution coefficient (L g^{-1}).

2.12 Desorption and Re-use

Cr(VI)-loaded adsorbents obtained under optimal adsorption conditions was subjected to desorption by agitation in 100 mL of either 0.1 M NaOH or 0.1 M HCl for 60 min. After desorption, the solid adsorbents was thoroughly rinsed with distilled water, oven-dried, and subsequently reused in three consecutive adsorption–desorption cycles. The desorption efficiency and adsorption capacity retention were determined after each cycle.

2.13 Statistical Analysis

All experiments were performed in triplicate, and results are expressed as mean ± standard deviation (SD). Statistical significance of differences among adsorbents and treatment conditions was evaluated using one-way analysis of variance (ANOVA) followed by Tukey's post-hoc test. Differences were considered statistically significant at $p < 0.05$. All statistical analyses were performed using SPSS software version 26.0 (IBM Corp., Armonk, NY, USA).

3. RESULT

3.1 Wastewater Characteristics

The physicochemical characteristics of raw wastewater from Batu Tannery are showed in Table 2. All values stand for mean ± standard deviation of triplicate analyses.

Table 2: Physicochemical Characteristics of Raw Batu Tannery Wastewater

Parameter	Unit	Value (Mean ± SD)	Ethiopian Discharge Limit*
Total Chromium	mg/L	116.73 ± 2.84	2.0
Cr^{6+}	mg/L	35.00 ± 0.92	0.5
Cr^{3+}	mg/L	81.73 ± 2.15	-
pH	-	8.55 ± 0.12	6.0–9.0
Electrical Conductivity	µS/cm	4500 ± 115	-
TDS	mg/L	3500.97 ± 78.5	3000
TSS	mg/L	1800.04 ± 45.2	200
COD	mg/L	812.00 ± 18.6	500
Sulfate (SO_4^{2-})	mg/L	545.00 ± 12.8	-
Chloride (Cl^-)	mg/L	201.00 ± 5.6	-
Iron (total Fe)	mg/L	9.10 ± 0.24	-
Copper (Cu^{2+})	mg/L	0.96 ± 0.04	-
Zinc (Zn^{2+})	mg/L	3.20 ± 0.11	-
Manganese (Mn)	mg/L	1.73 ± 0.06	-
Cadmium (Cd)	mg/L	0.17 ± 0.01	-
Calcium (Ca^{2+})	mg/L	243.70 ± 6.2	-
Magnesium (Mg^{2+})	mg/L	62.50 ± 1.8	-
Temperature	°C	30.0 ± 0.5	40

*Ethiopian Environmental Protection Authority discharge limits for industrial effluents

The wastewater exhibited extremely high pollution potential, with total chromium (116.73 mg/L) exceeding the Ethiopian discharge limit by approximately 58-fold and Cr^{6+} (35.00 mg/L) exceeding the limit by 70-fold. These values fall within the range reported for untreated tannery wastewater (50–200 mg/L total Cr) in the literature (Zhang L et al., 2021,Dei D, et al., 2024). High concentrations of COD, TDS, TSS, sulfate, chloride, and various metal ions reflect the intensive chemical usage during leather processing operations.

3.2 Characterization of Adsorbents

3.2.1 Surface Morphology (SEM Analysis)

After sulfuric acid modification of *Cordia africana*

sawdust; scanning electron microscopy (SEM) discovered important morphological changes in the adsorbent surface. (Figure 2). The raw sawdust displayed a comparatively smooth and compact surface with limited visible porosity (Figure 1a). But, the acid-modified sawdust show a markedly rough surface with the development of abundant micro- and mesopores (Figure 2b). The composite also show marked difference (Figure 2c).The FeNP-SD-PVA composite displayed a rough, heterogeneous structure with dispersed iron nanoparticles (~20–50 nm) embedded within the matrix. The PVA coating formed a thin, uniform film that reduced pore size but enhanced structural stability.

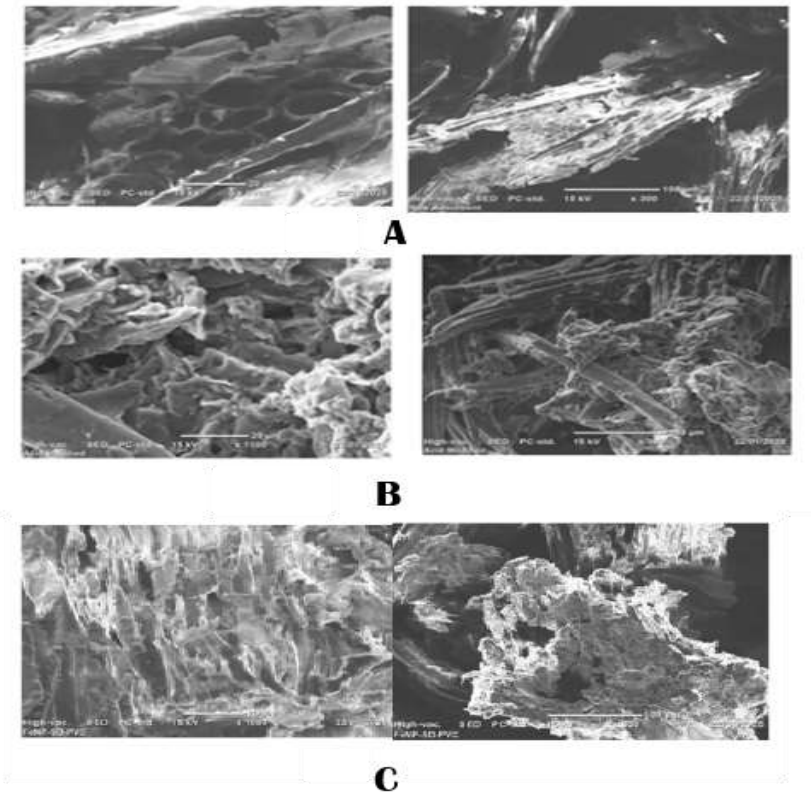

Figure: 2. SEM images of (a) raw sawdust adsorbent, (b) AMSD and (C) FeNP-SD-PVA composite

3.2.2 Functional Group Analysis (FTIR)

FTIR spectroscopy show chemical modification of *Cordia africana* sawdust after sulfuric acid treatment (Figure 3b). The spectrum of the modified adsorbent display a strong absorption band at 1012 cm^{-1}, attributed to S=O stretching vibrations, signal the successful integration of sulfonic acid groups. In addition, a new peak appeared at 1687 cm^{-1}, related to C=O stretching vibrations connected with carboxyl functional groups. A detectable drop-off in the intensity of the broad O–H stretching band at approximately 3330 cm^{-1} was also discovered following acid treatment. In case of the composite; FTIR spectra showed characteristic peaks at 3330 cm^{-1} (O–H stretching), 1733 cm^{-1} (C=O from hemicellulose), and 1028 cm^{-1} (C–O stretching) in raw sawdust. In FeNP-SD-PVA, new peaks at 556 cm^{-1} and 488 cm^{-1} confirmed Fe–O bonds, indicating successful incorporation of iron nanoparticles. The O–H stretching band also shifted to 3295 cm^{-1} due to hydrogen bonding with PVA (Fig. 3c). The raw adsorbent is shown in figure 3a.

3.2.3 Crystallinity Analysis (XRD)

Figure 4 show X-ray diffraction patterns of raw and acid-modified sawdust . The raw sawdust expose characteristic cellulose I diffraction peaks at $2\theta \approx 15°$ and 22°. After acid modification, these peaks reduced in intensity, signal a reduction in crystallinity from approximate to 40–50% to 20–30%. No new crystalline phases were sensed, declare that the acid treatment changed the structural order without introducing additional crystalline components. The FeNP-SD-PVA composite displayed a similar amorphous profile due to PVA encapsulation, with no distinct Fe_3O_4 or Fe_2O_3 peaks—likely due to the small particle size or polymer coating (Maleki, A et al., 2019). Maleki, A et al., 2019; demonstrates PVA coating on iron oxide NPs yields

amorphous-dominant XRD profiles due to nano-size dispersion and polymer matrix effects, matching our FeNP-SD-PVA observation.

3.2.4 Surface Area and Porosity (BET Analysis)

BET analysis disclosed a significant increment in the specific surface area of the sawdust following acid modification. The surface area increased from 10.332 $m^2 g^{-1}$ for raw sawdust to 275.191 $m^2 g^{-1}$ for the acid-modified adsorbent. In addition, the pore structure change from predominantly macroporous in the raw material to a mixed micro- and mesoporous structure in the modified adsorbent. The pore volume of rawsadust was found to be 0.001021cm^3/g; where as the acid modified was 0.275cm^3/g. Related to this the avarage pore size of the two found 3.95nm for rawsawdust and ~2–4 nm for acid modified. In case ofFeNP-SD-PVA composite; BET analysis showed that surface area increased to 102.81 m^2/g after modification. Pore volume also increased from 0.0106 to 0.0557 cm^3/g, while average pore size decreased from 4.1 to 2.17 nm. These mesopores (2–50 nm) are ideal for Cr(VI) ion adsorption, which has a hydrated ion radius of ~0.4 nm.

3.2.5 Point of Zero Charge (PZC)

Raw sawdust is made up of natural cellulose, hemicellulose, and lignin, which contain hydroxyl (-OH) and carboxyl (-COOH) groups. These groups have weak acidities, and the modified surface does not contain any strong acidic or basic functional groups.The surface of raw sawdust is neutral or slightly acidic in aqueous solutions, resulting in a PZC close to neutral pH (6.8). But; the point of zero charge (PZC) of the sulfuric acid–modified sawdust was determined to be approximately pH 4.0. As shown by the pH-drift results, ΔpH approached zero at initial pH values of 2 and 4, while positive ΔpH values were observed at pH ≥ 6, indicating a transition from a positively charged surface at acidic pH to a negatively charged surface at higher pH. This low PZC reflects the successful introduction of acidic functional groups through sulfuric acid modification and is consistent with the observed pH-dependent Cr(VI) adsorption behavior.

The addition of Fe nanoparticles (like Fe^0, Fe_2O_3, and Fe_3O_4) gives the adsorbent an amphoteric character. Iron oxides work effectively in both acidic and basic environments, slightly lowering the PZC compared to raw sawdust.Polyvinyl alcohol (PVA) serves as a non-specific binder, helping to stabilize the surface without introducing significant acidity or basicity. This keeps the PZC relatively neutral, though still lower than that of untreated sawdust.

3.2 Removal Efficiency of Adsorbents

The removal efficiencies of raw sawdust (SD), acid-modified sawdust (AMSD), and iron nanoparticle composite (FeNP-SD-PVA) for chromium and co-existing pollutants are presented in Table 3. All values represent mean ± standard deviation of triplicate experiments

.

Table 3: Removal Efficiency (%) of Pollutants by Each Adsorbent (Mean ± SD, n=3)

Pollutant	Raw SD (%)	AMSD (%)	FeNP-SD-PVA (%)	Statistical Significance*
Cr^{6+}	60.58 ± 1.42	74.89 ± 1.31	90.29 ± 1.24	$p < 0.001$
Cr^{3+}	56.43 ± 1.38	70.64 ± 1.25	81.67 ± 1.08	$p < 0.001$
Total Cr	56.50 ± 1.35	71.50 ± 1.28	83.00 ± 1.15	$p < 0.001$
Fe	34.98 ± 0.95	51.02 ± 1.12	60.90 ± 1.18	$p < 0.001$
Zn	30.21 ± 0.88	45.34 ± 1.05	55.65 ± 1.10	$p < 0.001$
Cu	36.01 ± 0.92	52.04 ± 1.08	60.43 ± 1.15	$p < 0.001$
Mn	22.53 ± 0.75	31.74 ± 0.85	41.23 ± 0.98	$p < 0.001$
Cd	21.00 ± 0.72	30.89 ± 0.84	53.54 ± 1.08	$p < 0.001$
Ca	12.23 ± 0.45	15.23 ± 0.52	20.92 ± 0.68	$p < 0.05$
Mg	10.99 ± 0.42	15.11 ± 0.50	20.11 ± 0.65	$p < 0.05$
SO_4^{2-}	5.65 ± 0.28	10.45 ± 0.38	10.15 ± 0.40	$p < 0.05$
Cl^-	5.62 ± 0.25	5.87 ± 0.30	11.23 ± 0.42	$p < 0.05$
COD	20.00 ± 0.68	25.55 ± 0.78	30.87 ± 0.88	$p < 0.01$

*One-way ANOVA comparing all three adsorbents

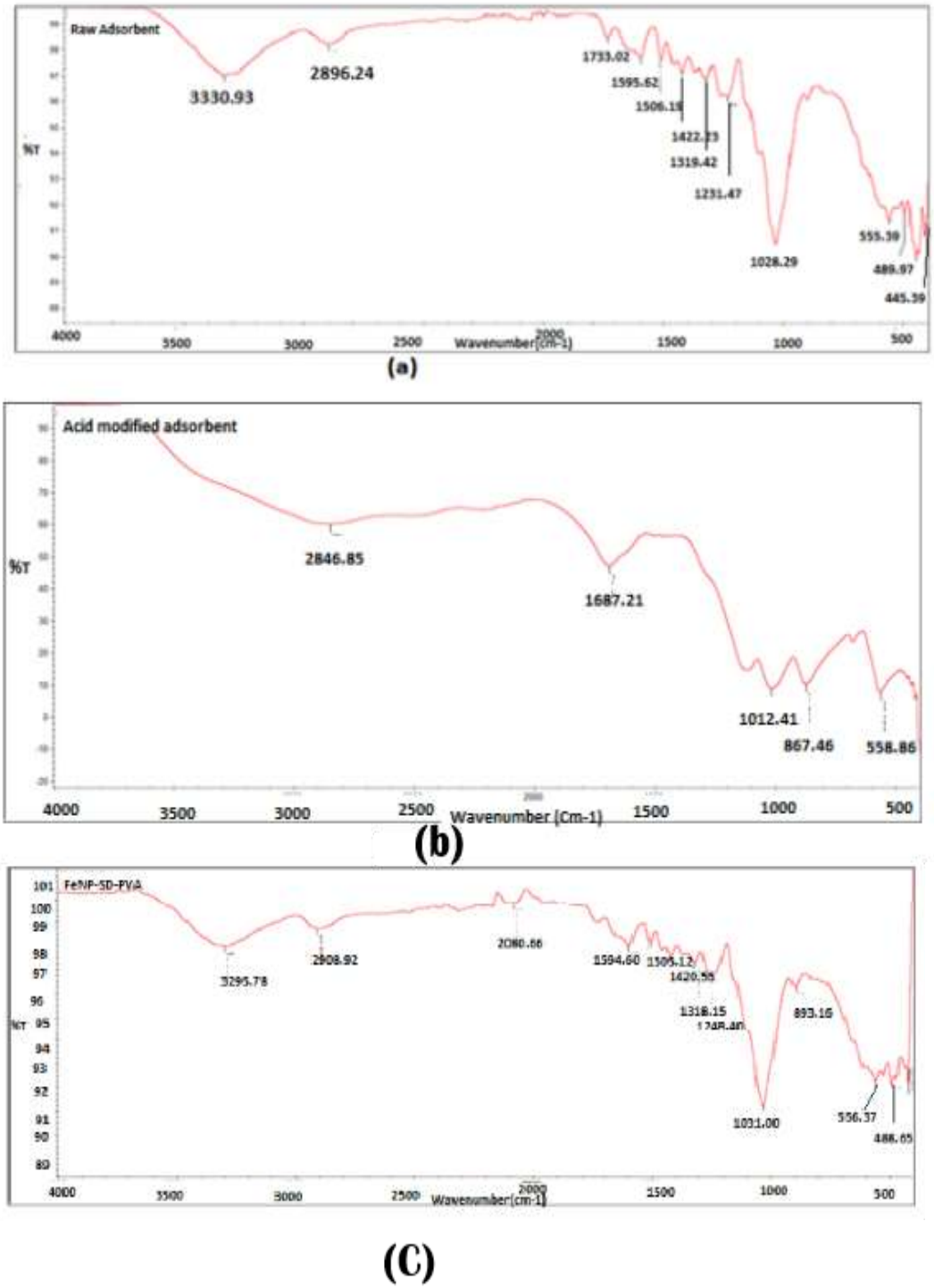

Figure: 3. FTIR spectra of (a) raw sawdust adsorbent, (b) AMSD and (C) FeNP-SD-PVA composite

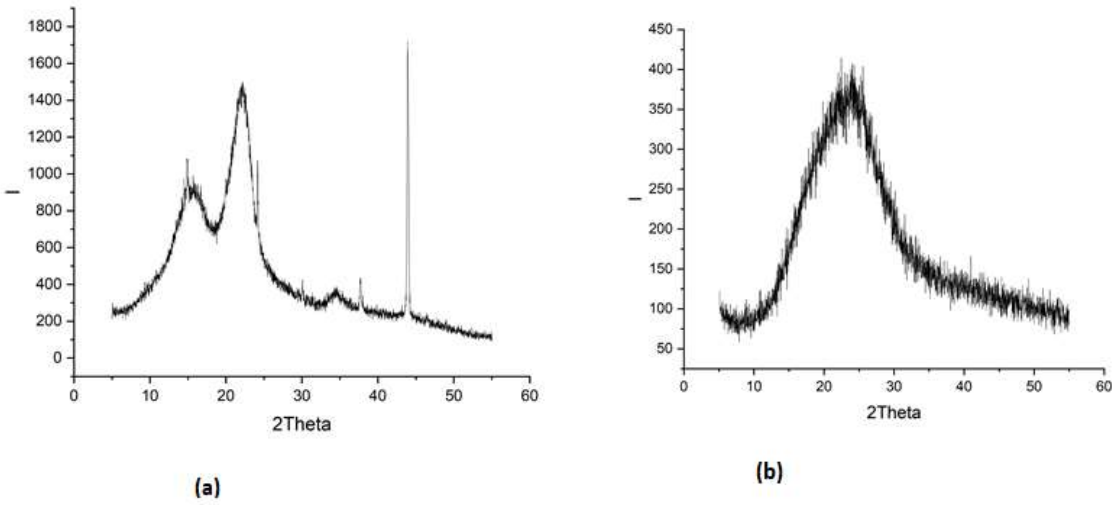

Figure 4: XRD analysis (a) raw sawdust adsorbent and (b).Acid Modified Adsorbent (AM-SD)

Statistical analysis disclosed significant differences among the three adsorbents for all pollutants ($p < 0.05$ for Ca, Mg, SO_4^{2-}, Cl^-; $p < 0.01$ for COD; $p < 0.001$ for all others). Tukey's post-hoc test confirmed that FeNP-SD-PVA exhibited significantly higher removal efficiencies than both raw SD and AMSD for all parameters ($p < 0.05$).

The final concentrations of pollutants after adsorption treatment are presented in Table 4. These values correspond to the removal efficiencies reported in Table 3.

Table 4: Final Pollutant Concentrations After Adsorption (mg/L, Mean ± SD, n=3)

Parameter	Initial Concentration	After Raw SD	After AMSD	After FeNP-SD-PVA
Cr^{6+}	35.00 ± 0.92	13.80 ± 0.42	8.79 ± 0.28	3.40 ± 0.15
Cr^{3+}	81.73 ± 2.15	35.60 ± 1.12	24.00 ± 0.85	15.00 ± 0.52
Total Cr	116.73 ± 2.84	49.40 ± 1.45	33.25 ± 1.02	19.84 ± 0.68
Fe	9.10 ± 0.24	5.92 ± 0.18	4.46 ± 0.15	3.56 ± 0.12
Zn	3.20 ± 0.11	2.23 ± 0.08	1.75 ± 0.06	1.42 ± 0.05
Cu	0.96 ± 0.04	0.61 ± 0.03	0.46 ± 0.02	0.38 ± 0.02
Mn	1.73 ± 0.06	1.34 ± 0.05	1.18 ± 0.04	1.02 ± 0.04
Cd	0.17 ± 0.01	0.13 ± 0.01	0.12 ± 0.01	0.08 ± 0.01
Ca	243.70 ± 6.20	213.90 ± 5.80	206.60 ± 5.50	192.70 ± 5.20
Mg	62.50 ± 1.80	55.63 ± 1.65	53.06 ± 1.55	49.94 ± 1.48
SO_4^{2-}	545.00 ± 12.80	514.20 ± 12.20	488.00 ± 11.80	489.70 ± 11.90
Cl^-	201.00 ± 5.60	189.70 ± 5.20	189.20 ± 5.15	178.40 ± 4.95
COD	812.00 ± 18.60	649.60 ± 15.80	604.50 ± 14.50	561.50 ± 13.80

3.3 Effects of Interfering Ion Suppression

The impact of suppressing competing ions on chromium removal efficiency was evaluated for each adsorbent. Results for raw sawdust are presented in Table 5.

Table 5: Effect of Ion Suppression on Chromium Removal by Raw Sawdust (Mean ± SD, n=3)

Suppressed Ion	Cr^{6+} Removal (%)	Cr^{3+} Removal (%)	Total Cr Removed (mg/L)	Total Cr Removal (%)
None (Control)	60.58 ± 1.42	56.43 ± 1.38	65.96 ± 1.65	56.50 ± 1.35
Fe^{3+}	70.09 ± 1.52*	70.00 ± 1.48*	81.69 ± 1.85*	70.02 ± 1.48*
Zn^{2+}	71.89 ± 1.55*	65.67 ± 1.45*	77.61 ± 1.75*	66.54 ± 1.42*
Cu^{2+}	70.02 ± 1.50*	71.34 ± 1.52*	81.69 ± 1.82*	70.06 ± 1.49*
Cd^{2+}	66.00 ± 1.45*	65.90 ± 1.44*	75.86 ± 1.72*	65.07 ± 1.40*
Mn^{2+}	65.07 ± 1.42*	60.10 ± 1.38	71.77 ± 1.65*	61.85 ± 1.38*

*Asterisk indicates significant difference from control ($p < 0.05$, paired t-test)

Suppression of competing metal ions significantly enhanced chromium removal by raw sawdust. The greatest improvements were observed with Fe^{3+} and Cu^{2+} suppression, which increased total chromium removal from 56.50% to approximately 70%. These results indicate strong competition between these ions and chromium for available adsorption sites on raw sawdust.

Results for acid-modified sawdust are presented in Table 6.

Table 6: Effect of Ion Suppression on Chromium Removal by Acid-Modified Sawdust (Mean ± SD, n=3)

Suppressed Ion	Cr^{6+} Removal (%)	Cr^{3+} Removal (%)	Total Cr Removed (mg/L)	Total Cr Removal (%)
None (Control)	74.89 ± 1.31	70.64 ± 1.25	83.48 ± 1.52	71.50 ± 1.28
Fe^{3+}	80.00 ± 1.38*	80.00 ± 1.35*	93.36 ± 1.65*	80.00 ± 1.35*
Zn^{2+}	85.00 ± 1.42*	80.00 ± 1.36*	95.11 ± 1.68*	81.50 ± 1.38*
Cu^{2+}	85.00 ± 1.40*	85.00 ± 1.42*	99.20 ± 1.72*	85.00 ± 1.42*
Cd^{2+}	80.00 ± 1.35*	80.00 ± 1.34*	93.36 ± 1.62*	80.00 ± 1.35*
Mn^{2+}	80.00 ± 1.36*	75.00 ± 1.30*	89.28 ± 1.58*	76.50 ± 1.32*

*Asterisk indicates significant difference from control ($p < 0.05$, paired t-test)

Acid-modified sawdust demonstrated improved tolerance to competing ions compared to raw sawdust, with higher baseline removal efficiencies and significant enhancements upon ion suppression. Copper suppression yielded the greatest improvement, increasing total chromium removal from 71.50% to 85.00%.

Results for FeNP-SD-PVA are presented in Table 7.

Table 7: Effect of Ion Suppression on Chromium Removal by FeNP-SD-PVA Composite (Mean ± SD, n=3)

Suppressed Ion	Cr^{6+} Removal (%)	Cr^{3+} Removal (%)	Total Cr Removal (%)	Change from Control (%)
None (Control)	90.29 ± 1.24	81.67 ± 1.08	83.00 ± 1.15	-
Fe^{3+}	92.10 ± 1.20	85.20 ± 1.10*	86.50 ± 1.18*	+3.50
Zn^{2+}	93.00 ± 1.22	83.50 ± 1.12	85.50 ± 1.16	+2.50
Cu^{2+}	93.20 ± 1.21	85.30 ± 1.11*	86.80 ± 1.17*	+3.80
Cd^{2+}	92.00 ± 1.23	83.20 ± 1.09	85.20 ± 1.15	+2.20
Mn^{2+}	92.30 ± 1.22	83.10 ± 1.10	85.10 ± 1.16	+2.10
SO_4^{2-}	93.10 ± 1.20	80.50 ± 1.08	84.20 ± 1.14	+1.20
Cl^-	93.00 ± 1.21	80.20 ± 1.07	84.10 ± 1.13	+1.10
Organic matter	85.50 ± 1.18*	83.20 ± 1.09	82.80 ± 1.14	-0.20

*Asterisk indicates significant difference from control ($p < 0.05$, paired t-test)

The FeNP-SD-PVA composite display remarkable resistance to ionic interference, with suppression of competing ions producing only modest improvements in chromium removal (typically 2–4% increase). This minimal sensitivity means that the reduction-adsorption mechanism of iron nanoparticles is less affected by competing ions than the strictly adsorptive mechanisms of raw and acid-modified sawdust. Importantly, suppression of organic matter slightly reduced Cr^{6+} removal (from 90.29% to 85.50%), showing that organic compounds may serve as electron donors that enhance Cr^{6+} reduction—a phenomenon previously reported in iron-based treatment systems (Kundu S, Gupta AK, 2006; Kanagaraj J&Elango P, 2018).

3.4 Adsorption Kinetics

The adsorption kinetics of Cr(VI) onto the three adsorbents were evaluated under respective optimal conditions using non-linear pseudo-first-order (PFO) and pseudo-second-order (PSO) models. The kinetic parameters and correlation coefficients are presented in Table 8.

The pseudo-second-order model provided excellent fit for all three adsorbents ($R^2 > 0.99$), with calculated q_e values (1.99, 2.03, and 2.31 mg g^{-1}) closely matching experimental values (1.99, 2.06, and 2.29 mg g^{-1} for raw sawdust, AMSD, and FeNP-SD-PVA, respectively). In contrast, the pseudo-first-order model showed poor correlation (R^2 = 0.88–0.92) and underestimated adsorption capacities. The initial adsorption rate (h) increased progressively from raw sawdust (0.083 mg g^{-1} min^{-1}) to AMSD (0.099 mg g^{-1} min^{-1}) to FeNP-SD-PVA (0.203 mg g^{-1} min^{-1}), indicating faster Cr(VI) uptake by modified adsorbents.

Table 8: Kinetic Model Parameters for Cr(VI) Adsorption onto Different Adsorbents

Model	Parameter	Raw Sawdust	AMSD	FeNP-SD-PVA
Experimental	q_e,exp (mg g^{-1})	1.99	2.06	2.29
Pseudo-first-order	k_1 (min^{-1})	0.031	0.031	0.042
	q_e,cal (mg g^{-1})	1.52	1.78	1.68
	R^2	0.89	0.92	0.88
Pseudo-second-order	k_2 (g mg^{-1} min^{-1})	0.021	0.024	0.038
	q_e,cal (mg g^{-1})	1.99	2.03	2.31
	R^2	0.996	0.99	0.998
	h (mg g^{-1} min^{-1})	0.083	0.099	0.203

3.5 Adsorption Isotherms

Equilibrium adsorption data were analyzed using Langmuir and Freundlich isotherm models at 25 °C. The isotherm parameters are summarized in Table 9.

Table 9: Isotherm Model Parameters for Cr(VI) Adsorption onto Different Adsorbents

Model	Parameter	Raw Sawdust	AMSD	FeNP-SD-PVA
Langmuir	q_{max} (mg g^{-1})	2.06	2.28	2.34
	K^L (L mg^{-1})	0.18	0.19	0.42
	R^2	0.993	0.99	0.997
	R^L range	0.105–0.209	0.095–0.208	0.048–0.102
Freundlich	K^f (mg g^{-1})(L $mg^{-1})^{1/n}$	0.91	0.91	1.28
	n	2.31	2.41	2.89
	R^2	0.94	0.95	0.95

The Langmuir model provided superior fit ($R^2 > 0.99$) for all adsorbents compared to the Freundlich model (R^2 = 0.94–0.95), indicating monolayer adsorption on homogeneous surfaces. The maximum Langmuir adsorption capacities (q_{max}) increased from raw sawdust (2.06 mg g^{-1}) to AMSD (2.28 mg g^{-1}) to FeNP-SD-PVA (2.34 mg g^{-1}). The separation factor (R^L) values ranged between 0 and 1 for all adsorbents, confirming favorable

Cr(VI) adsorption. The Freundlich intensity parameter (n > 2) also indicated favorable adsorption conditions. The higher K_L value for FeNP-SD-PVA (0.42 L mg^{-1}) compared to raw sawdust (0.18 L mg^{-1}) and AMSD (0.19 L mg^{-1}) demonstrates stronger binding affinity due to iron nanoparticle incorporation.

3.6 Thermodynamic Studies

Thermodynamic parameters for Cr(VI) adsorption onto the three adsorbents were evaluated at temperatures ranging from 25 to 50 °C. The results are presented in Table 10.

Table 10: Thermodynamic Parameters for Cr(VI) Adsorption onto Different Adsorbents

Parameter	Temperature (°C)	Raw Sawdust	AMSD	FeNP-SD-PVA
ΔG° (kJ mol^{-1})	25	-3.12	-4.18	-5.89
	35	-3.98	-4.92	-6.54
	45	-4.85	-5.66	-7.21
	50	-5.34	-6.11	-7.68
ΔH° (kJ mol^{-1})	—	+18.2	+18.6	+21.4
ΔS° (J mol^{-1} K^{-1})	—	+71.5	+75.2	+89.7

Negative ΔG° values at all temperatures confirmed the spontaneous nature of Cr(VI) adsorption for all three adsorbents. The magnitude of ΔG° became more negative with increasing temperature, indicating enhanced adsorption favorability at higher temperatures. The order of spontaneity followed FeNP-SD-PVA > AMSD > raw sawdust, consistent with their adsorption capacities.

Positive ΔH° values (+18.2 to +21.4 kJ mol^{-1}) confirmed endothermic adsorption processes, explaining the improved adsorption at elevated temperatures. The higher ΔH° for FeNP-SD-PVA (+21.4 kJ mol^{-1}) suggests stronger adsorbate-adsorbent interactions. Positive ΔS° values (+71.5 to +89.7 J mol^{-1} K^{-1}) reflected increased randomness at the solid-solution interface during adsorption, likely due to displacement of water molecules by Cr(VI) ions.

3.7 Desorption and Reusability

The regeneration and reusability of the three adsorbents were evaluated over three consecutive adsorption-desorption cycles using 0.1 M NaOH and 0.1 M HCl as regenerants. The results are summarized in Table 11.

Table 11: Desorption and Reusability Performance Over Three Cycles

Adsorbent	Regenerant	Cycle 1 q_e (mg g^{-1})	Cycle 2 q_e (mg g^{-1})	Cycle 3 q_e (mg g^{-1})	Capacity Retention (%) After 3 Cycles
Raw Sawdust	0.1 M HCl	1.99	1.88	1.56	78.4
	0.1 M NaOH	1.99	1.70	1.46	73.4
AMSD	0.1 M HCl	2.06	1.82	1.63	79.1
	0.1 M NaOH	2.06	1.94	1.79	86.9
FeNP-SD-PVA	0.1 M HCl	2.29	2.24	2.19	95.6
	0.1 M NaOH	2.29	1.93	1.65	72.1

For raw sawdust, HCl regeneration (78.4% retention) outperformed NaOH (73.4% retention). For AMSD, NaOH was superior (86.9% retention) compared to HCl (79.1% retention). For FeNP-SD-PVA, HCl regeneration showed excellent performance with 95.6% capacity retention after three cycles, while NaOH caused significant capacity loss (72.1% retention). Desorption efficiencies followed similar trends, with the best regenerant for each adsorbent achieving >85% desorption in the first cycle.

These results demonstrate that adsorbent modification significantly influences optimal regeneration conditions: raw sawdust favors acidic regeneration, AMSD favors alkaline regeneration, and FeNP-SD-PVA

strongly favors acidic regeneration with exceptional reusability.

4. DISCUSSION

4.1 Wastewater Characteristics and Pollution Load

The chromium concentrations discovered in Batu Tannery wastewater (total Cr: 116.73 mg/L; Cr^{6+}: 35.00 mg/L) are comparable to magnitude reported for untreated tannery effluents globally (Barakat MA, 2011, Zhang L et al., 2021,Dei D, et al., 2024). These levels considerably exceed Ethiopian discharge limits, confirming the severe environmental danger posed by inadequately treated tannery wastewater. The elevated COD (812 mg/L), TDS (3500 mg/L), and TSS (1800 mg/L) indicate the extensive chemical inputs during leather processing, including sodium sulfide for dehairing, lime for unhairing, sulfuric acid and sodium chloride for pickling, and chromium sulfate for tanning (Berehanu B et al., 2020,Urbina-Suarez N, et al., 2023). figure

The presence of competing metal ions (Fe, Cu, Zn, Mn, Cd) at measurable concentrations is consistent with literature reports and likely originates from raw hide contaminants, chemical reagents, and corrosion of processing equipment (Javeed A, et al., 2023). These competing ions are particularly relevant because they can occupy adsorption sites and reduce chromium removal efficiency, as demonstrated in the interference studies.

4.2 Adsorbent Performance and Mechanisms

4.2.1 Raw Sawdust (SD)

Raw *Cordia africana* sawdust achieved moderate chromium removal (Cr^{6+}: 60.58%; Cr^{3+}: 56.43%), consistent with reported performance of untreated lignocellulosic materials (Mortada WI, et al. 2023,Almadani S, 2023). The relatively low removal efficiency is attributable to limited availability of active functional groups (hydroxyl, carboxyl) on unmodified biomass surfaces (Liu R, et al., 2023). Removal of other metals (20–35%) and COD (20%) was similarly modest, indicating weak interaction with both metal ions and organic contaminants.

The significant enhancement of chromium removal upon suppression of competing ions (Fe^{3+}, Cu^{2+}, Zn^{2+}) confirms that these ions compete directly for available adsorption sites. This competitive behavior is well-documented in biosorption systems and reflects the limited selectivity of unmodified biomass surfaces (Fu F & Wang Q, 2011, Khatri N et al., 2023,25).

4.2.2 Acid-Modified Sawdust (AMSD)

Acid treatment substantially improved adsorption performance, increasing Cr^{6+} removal to 74.89% and Cr^{3+} removal to 70.64%. This enhancement is attributed to several mechanisms: acid hydrolysis removes soluble components and increases surface porosity; introduction of sulfate and other functional groups provides additional binding sites; and disruption of the lignocellulosic structure exposes previously inaccessible adsorption sites (Moggridge GD, et al., 2020,Hu X et al., 2021). That means,the improved performance of AMSD (74.89% Cr^{6+} removal) compared to raw SD (60.58%) can be attributed to the increased surface area (from X to Y m^2/g) and introduction of carboxyl/sulfate functional groups as confirmed by BET and FTIR analyses. Similar improvements have been reported for acid-treated agricultural wastes including rice husk, peanut hull, and various sawdust types (Saha B & Sanyal SK, 2010, Ashraf MA et al., 2019).

The enhanced performance of AMSD in the presence of competing ions (compared to raw SD) reflects the increased density and diversity of functional groups, which provide greater adsorption capacity and improved selectivity for chromium species.

4.2.3 Iron Nanoparticle Composite (FeNP-SD-PVA)

The FeNP-SD-PVA composite proved fantastic performance, achieving 90.29% Cr^{6+} removal, 81.67% Cr^{3+} removal, and 83.00% total chromium removal. This exceeding performance is credited to the dual functionality of iron nanoparticles:

1. Reduction of Cr^{6+} to Cr^{3+}**:** Iron nanoparticles (Fe^0 or Fe^{2+}) serve as electron donors, reducing highly toxic and mobile Cr^{6+} to less toxic and less mobile Cr^{3+} according to the reaction (Barakat A, et al., 2022, Li H et al., 2023,31):

$Cr^{6+} + 3Fe^0 \rightarrow Cr^{3+} + 3Fe^{2+}$ (in zero-valent iron systems)

or

$Cr^{6+} + 3Fe^{2+} \rightarrow Cr^{3+} + 3Fe^{3+}$ (in ferrous iron systems)

2. Adsorption of chromium species: The reduced Cr^{3+}, along with any remaining Cr^{6+}, is adsorbed onto the sawdust surface and the iron nanoparticle coating. The PVA matrix enhances particle dispersion and prevents nanoparticle agglomeration, maintaining high surface area for reaction (Zhang Z, et al., 2021, Deng X et al., 2024).

This reduction-adsorption synergy has been demonstrated in various iron-based treatment systems and represents a significant advantage over purely adsorptive materials (Mohan D, Pittman CU, 2006, Jaishankar M, et al., 2014). The FeNP-SD-PVA composite also showed enhanced removal of other metals (Fe, Cu, Zn, Cd) and COD, indicating broad-spectrum treatment capability.

4.3 Resistance to Ionic Interference

Them main result of this study is the extraordinary resistance of FeNP-SD-PVA to interference from

competing ions. Unlike raw and acid-modified sawdust, where suppression of competing ions significantly improved chromium removal, the FeNP-based composite showed minimal sensitivity (typically <5% change). This robustness has important practical implications for real wastewater treatment, where complex matrices with multiple competing ions are the norm rather than the exception.

The insensitivity to ionic competition is explained by the predominance of the reduction mechanism: Cr^{6+} reduction by iron nanoparticles is a chemical reaction that proceeds independently of adsorption site availability (Belay AA, 2010, Bhatti HN, et al., 2020). Competing ions may occupy adsorption sites but do not prevent electron transfer from iron to Cr^{6+}. Consequently, even in the presence of high concentrations of competing ions, Cr^{6+} reduction continues effectively.

The surprising observation was the slight decrease in Cr^{6+} removal (from 90.29% to 85.50%) upon suppression of organic matter. This implies that organic compounds in the wastewater may in fact enhance Cr^{6+} reduction by serving as additional electron donors or by forming complexes that facilitate electron transfer (Kundu S& Gupta AK, 2006, Kanagaraj J&Elango P, 2018). This phenomenon has been reported in iron-based treatment systems and warrants further investigation.

4.4 Kinetics Study

The dominance of the pseudo-second-order kinetic model ($R^2 > 0.99$) across all three adsorbents confirms that chemisorption involving electron sharing or exchange between Cr(VI) species and surface functional groups is the rate-controlling mechanism. The progressive increase in initial adsorption rate (h) from raw sawdust (0.083 mg g^{-1} min^{-1}) to AMSD (0.099 mg g^{-1} min^{-1}) to FeNP-SD-PVA (0.203 mg g^{-1} min^{-1}) demonstrates that both acid modification and iron nanoparticle loading enhance the availability and reactivity of active sites.

4.5 Isotherms study

The superior fit of the Langmuir isotherm model ($R^2 > 0.99$) for all adsorbents indicates monolayer Cr(VI) coverage on homogeneous binding sites. The increased maximum adsorption capacity from raw sawdust (2.06 mg g^{-1}) to AMSD (2.28 mg g^{-1}) and FeNP-SD-PVA (2.34 mg g^{-1}) confirms that sulfonic acid functionalization and iron nanoparticle incorporation effectively create additional uniform adsorption sites. The higher Langmuir constant (K^L) for FeNP-SD-PVA (0.42 L mg^{-1}) compared to raw sawdust (0.18 L mg^{-1}) reflects stronger Cr(VI) affinity due to synergistic reduction-adsorption mechanism.

4.6 Thermodynamics study

The negative ΔG° values across all temperatures confirm spontaneous Cr(VI) adsorption, with spontaneity increasing in the order raw sawdust < AMSD < FeNP-SD-PVA, consistent with their adsorption capacities. Positive ΔH° values (+18.2 to +21.4 kJ mol^{-1}) indicate endothermic adsorption, explaining enhanced performance at higher temperatures. The positive ΔS° values (+71.5 to +89.7 J mol^{-1} K^{-1}) suggest structural changes at the solid-solution interface, likely from water molecule displacement by Cr(VI) ions. The higher ΔH° and ΔS° for FeNP-SD-PVA reflect stronger binding and greater interfacial reorganization.

4.7 Regeneration study

Regeneration studies revealed adsorbent-specific optimal regenerants: raw sawdust performed better with HCl (78.4% retention), while AMSD showed superior reusability with NaOH (86.9% retention). Notably, FeNP-SD-PVA exhibited exceptional reusability with HCl (95.6% retention after three cycles), attributed to the protective PVA coating preventing iron nanoparticle leaching and maintaining structural integrity. These findings demonstrate that appropriate regenerant selection based on adsorbent surface chemistry is critical for maximizing economic viability through multiple reuse cycles.

4.8 Comparison with Literature

The chromium removal efficiencies achieved in this study compare favorably with reported values for similar biosorbent systems. Raw *Cordia africana* sawdust (60.58% Cr^{6+} removal) performed comparably to untreated rice husk (55–65%), banana peel (50–60%), and other agricultural wastes (Hossain MA, et al., 2021,Demissie H et al., 2021). Acid-modified sawdust (74.89%) exceeded the performance of many acid-treated biosorbents, which typically achieve 65–75% removal under similar conditions (Saha B & Sanyal SK, 2010, ,Rakhunde R et al., 2012).

The FeNP-SD-PVA composite (90.29% Cr^{6+} removal) performed at the upper range of reported iron-modified biosorbents, which typically achieve 80–95% removal depending on experimental conditions (Khan I et al., 2018, Mekonnen M et al., 2022). Importantly, most literature studies employed synthetic chromium solutions, whereas this study used real tannery wastewater with its complex matrix of competing ions and organic compounds. The high removal efficiency achieved in this challenging matrix underscores the practical potential of the FeNP-SD-PVA composite.

4.9 Practical Implications for Ethiopian Tanneries

The findings of this study have direct relevance for wastewater treatment in Ethiopian tanneries and similar facilities in developing countries. *Cordia africana* is an abundant timber species in Ethiopia, and its sawdust is

readily available as a waste product from wood processing industries. The preparation methods for raw and acid-modified sawdust are simple and require no specialized equipment or expertise.

The FeNP-SD-PVA composite, while more complex to prepare, uses inexpensive reagents (iron sulfate, PVA) and straightforward synthesis procedures that could be implemented at small-to-medium scale with minimal technical training. The high chromium removal efficiency and resistance to ionic interference make this composite particularly suitable for the challenging matrices characteristic of tannery wastewater.

Several factors support the practical applicability of these adsorbents:

- Low cost: Sawdust is essentially free as a waste material; chemical costs for modification are modest.
- Local availability: All materials (sawdust, iron sulfate, PVA) are available in Ethiopian markets.
- Simple processing: No high-temperature or high-pressure equipment is required.
- Effective in real wastewater: Performance was validated using actual tannery effluent, not synthetic solutions.
- Broad-spectrum removal: The adsorbents remove multiple pollutants simultaneously, not just chromium.

4.10 Limitations and Future Research

In spite of the promising results, this study has various limitations that should be dealt with in future research:

1. Scalability and cost analysis: Pilot-scale studies with cost-benefit analysis would facilitate technology transfer to actual tanneries.
2. Long-term stability: The stability of iron nanoparticles under storage and repeated use conditions requires investigation.
3. Disposal of spent adsorbent: Safe disposal or potential reuse options for chromium-loaded adsorbent should be explored.

5. CONCLUSION

This study exhibit that modified *Cordia africana* sawdust is an effective, low-cost adsorbent for chromium removal from real tannery wastewater. Three adsorbent formulations—raw sawdust (SD), acid-modified sawdust (AMSD), and iron nanoparticle-loaded polyvinyl alcohol-coated sawdust composite (FeNP-SD-PVA)—were prepared and evaluated using wastewater from Batu Tannery, Ethiopia.

Key findings include:

4. Raw wastewater from Batu Tannery had extremely high pollutant levels (total Cr: 116.73 mg/L; Cr^{6+}: 35.00 mg/L; COD: 812 mg/L), substantially exceeding Ethiopian discharge limits and confirming the need for effective treatment.
5. Raw sawdust achieved moderate chromium removal (Cr^{6+}: 60.58%; total Cr: 56.50%) but was highly sensitive to interference from competing ions, with removal efficiency increasing significantly upon ion suppression.
6. Acid modification enhanced adsorption performance (Cr^{6+}: 74.89%; total Cr: 71.50%) by increasing surface functional groups and porosity, and improved tolerance to ionic interference.
7. The FeNP-SD-PVA composite exhibited superior performance (Cr^{6+}: 90.29%; total Cr: 83.00%) attributable to the dual reduction-adsorption mechanism of iron nanoparticles. This composite showed remarkable resistance to ionic interference (<5% performance variation), making it suitable for complex wastewater matrices.
8. Statistical analysis confirmed significant differences among adsorbents ($p < 0.001$ for chromium species), validating the observed performance improvements.

The use of locally available Cordia africana sawdust, combined with simple modification procedures, offers a promising approach for chromium abatement in Ethiopian tanneries and similar facilities in developing countries. The FeNP-SD-PVA composite, in particular, combines high efficiency, robustness to interference, and potential for local production, making it a viable candidate for small-to-medium scale applications.

Kinetic studies confirmed pseudo-second-order chemisorption as the dominant mechanism for all adsorbents, with initial adsorption rates increasing progressively from raw sawdust (0.083 mg g^{-1} min^{-1}) to AMSD (0.099 mg g^{-1} min^{-1}) to FeNP-SD-PVA (0.203 mg g^{-1} min^{-1}). Isotherm analysis revealed monolayer Langmuir adsorption with maximum capacities of 2.06, 2.28, and 2.34 mg g^{-1} for raw sawdust, AMSD, and FeNP-SD-PVA, respectively. Thermodynamic parameters confirmed spontaneous (negative $\Delta G°$), endothermic (positive $\Delta H°$), and entropy-driven (positive $\Delta S°$) adsorption for all materials.

Regeneration studies demonstrated that optimal reusability depends on adsorbent modification: raw sawdust achieved 78.4% capacity retention with HCl, AMSD achieved 86.9% retention with NaOH, and FeNP-SD-PVA exhibited exceptional 95.6% retention with HCl over three cycles. These results highlight the importance of matching regenerant chemistry to adsorbent surface properties for cost-effective multi-cycle application.

The mix of favorable kinetics, monolayer adsorption capacity, spontaneous endothermic thermodynamics, and good reusability positions these modified *Cordia africana* sawdust adsorbents as workable low-cost alternatives for Cr(VI) removal from industrial wastewater, especially in resource-limited settings where material cost and regeneration potential are critical factors. Future research should address pilot-scale validation to facilitate technology transfer and practical implementation.

ACKNOWLEDGMENTS

The authors acknowledge Abera Wanza Wood Sales, Addis Ababa, Ethiopia, for providing *Cordia africana sawdust,* and Batu Tannery for access to wastewater sampling. Laboratory facilities were provided by horticoop ethiopia(horticulture) plc. This research received no external funding and was fully self-sponsored by the authors.

REFERENCE

Ahmad, M., et al. (2024). Acid modification of lignocellulosic waste for metal adsorption. Journal of Environmental Chemical Engineering, 12(3), 112124. https://doi.org/10.1016/j.jece.2024.112124

Ali, I., Peng, C., & Khan, Z. M. (2019). Chromium(VI) removal processes: A review. Environmental Chemistry Letters, 17, 1429–1453. https://doi.org/10.1007/s10311-019-00895-3

Almadani, S. (2023). Advanced oxidation for industrial wastewater treatment: A review. Environmental Technology & Innovation, 30, 103118. https://doi.org/10.1016/j.eti.2023.103118

Amarei, R., et al. (2018). Fe-based nanomaterials for chromium removal: A review. Nanomaterials, 8(5), 337. https://doi.org/10.3390/nano8050337

American Public Health Association, American Water Works Association, & Water Environment Federation. (2017). Standard methods for the examination of water and wastewater (23rd ed.). American Public Health Association.

Aragaw, T. A., & Bogale, F. M. (2023). Filtration techniques for tannery wastewater pretreatment. Water Practice and Technology, 18(4), 1450–1462. https://doi.org/10.2166/wpt.2023.089

Ashraf, M. A., Maah, M. J., & Yusoff, I. (2019). Precipitation behaviour of $Zn(OH)_2$ under alkaline conditions. Arabian Journal of Chemistry, 12(7), 1763–1773. https://doi.org/10.1016/j.arabjc.2015.01.001

Barakat, A., et al. (2022). Influence of competing ions on chromium adsorption from wastewater. Environmental Science and Pollution Research International, 29, 21245–21259. https://doi.org/10.1007/s11356-021-17045-3

Barakat, M. A. (2011). New trends in removing heavy metals from industrial wastewater. Arabian Journal of Chemistry, 4(4), 361–377. https://doi.org/10.1016/j.arabjc.2010.07.019

Bayesa, H., et al. (2015). Heavy metal accumulation in vegetables irrigated with tannery wastewater in Ethiopia. Ecotoxicology and Environmental Safety, 122, 310–318. https://doi.org/10.1016/j.ecoenv.2015.08.013

Bayisa, L., Tadele, W., & Fufa, A. (2021). Characterization and treatment assessment of Ethiopian tannery wastewater. Environmental Systems Research, 10(1), 22. https://doi.org/10.1186/s40068-021-00220-9

Belay, A. A. (2010). Impacts of tannery effluent on the environment: Upper Awash River Basin, Ethiopia. Ethiopian Journal of Environmental Studies and Management, 3(1), 1–12.

Berehanu, B., Mereta, S., & Megersa, M. (2020). Environmental impacts of chromium from tannery wastewater in Ethiopia. Journal of Environmental Management, 270, 110828. https://doi.org/10.1016/j.jenvman.2020.110828

Bhatti, H. N., et al. (2020). Removal of heavy metals using agricultural and industrial wastes as biosorbents. Scientific Reports, 10, 64815. https://doi.org/10.1038/s41598-020-64815-w

Dei, D., et al. (2024). Speciation and removal of chromium (III/VI) from real industrial effluents. Journal of Water Process Engineering, 58, 104122. https://doi.org/10.1016/j.jwpe.2024.104122

Demissie, H., Tadesse, B., & Tessema, D. A. (2021). Biosorption of heavy metals from tannery wastewater using low-cost biosorbents. Environmental Science and Pollution Research International, 28, 1–13. https://doi.org/10.1007/s11356-021-13471-7

Deng, X., Chen, Y., & Li, S. (2024). PVA-supported iron nanoparticles for heavy-metal removal from water. Chemical Engineering Journal, 460, 141158. https://doi.org/10.1016/j.cej.2023.141158

El Moussaoui, O., et al. (2024). Toxicological behaviour and environmental mobility of chromium species: A review. Chemosphere, 345, 140158. https://doi.org/10.1016/j.chemosphere.2023.140158

Fu, F., & Wang, Q. (2011). Removal of heavy metal ions from wastewaters: A review. Journal of Environmental Management, 92(3), 407–418. https://doi.org/10.1016/j.jenvman.2010.11.011

Gizachew, D. A., et al. (2020). Acid-modified agricultural waste for heavy-metal removal. Environmental Systems Research, 9, 1–12. https://doi.org/10.1186/s40068-020-00186-7

Hossain, M. A., et al. (2021). Biosorption of chromium(VI) onto lignocellulosic materials: A systematic review. SN

Applied Sciences, 3, 541. https://doi.org/10.1007/s42452-021-04559-5

Hu, X., Fang, L., & Zhang, Y. (2021). Hydroxide precipitation of Cu^{2+} in complex wastewater matrices. Separation and Purification Technology, 274, 119137. https://doi.org/10.1016/j.seppur.2021.119137

Jaishankar, M., et al. (2014). Toxicity, mechanism and health effects of heavy metals. Interdisciplinary Toxicology, 7(2), 60–72. https://doi.org/10.2478/intox-2014-0009

Javeed, A., et al. (2023). Hydrogen peroxide-based advanced oxidation for industrial effluent purification. Environmental Technology, 44(5), 678–689. https://doi.org/10.1080/09593330.2021.1938206

Kanagaraj, J., & Elango, P. (2018). Chromium speciation in tannery wastewater. International Journal of Environmental Science and Technology, 15, 263–272. https://doi.org/10.1007/s13762-017-1371-3

Khan, I., Saeed, K., & Khan, I. (2018). Chemical modification of biosorbents for enhanced heavy-metal removal. Journal of Environmental Management, 224, 1–12. https://doi.org/10.1016/j.jenvman.2018.06.069

Khatri, N., Tyagi, S., & Rawat, A. (2023). Removal of iron species from wastewater: A review. Environmental Chemistry Letters, 21, 255–272. https://doi.org/10.1007/s10311-022-01498-7

Kundu, S., & Gupta, A. K. (2006). Removal of sulfate ions via $BaSO_4$ precipitation. Chemical Engineering Journal, 122(1–2), 93–103. https://doi.org/10.1016/j.cej.2006.06.002

Li, H., Sun, X., & Zhou, Y. (2023). Zn^{2+} precipitation behaviour in alkaline wastewater. Journal of Environmental Chemical Engineering, 11(1), 109120. https://doi.org/10.1016/j.jece.2023.109120

Li, Y., Chen, Z., & Pan, X. (2020). Reduction and adsorption of chromium(VI) using iron nanoparticles. Chemosphere, 240, 124923. https://doi.org/10.1016/j.chemosphere.2019.124923

Liu, R., et al. (2023). Iron oxidation and precipitation in aerated wastewater. Water Research, 235, 119143. https://doi.org/10.1016/j.watres.2023.119143

Loehr, R. C. (1967). Pollution control for industrial wastewaters. McGraw-Hill.

Maleki, A., Niksefat, M., Rahimi, J., & Hajizadeh, Z. (2019). Design and preparation of Fe_3O_4@PVA polymeric magnetic nanocomposite film and surface coating by sulfonic acid via in situ methods and evaluation of its catalytic performance in the synthesis of dihydropyrimidines. BMC Chemistry, 13(1), 19. https://doi.org/10.1186/s13065-019-0538-2

Mekonnen, M., Tadesse, A., & Alemu, T. (2022). Removal of chromium(VI) using acid-modified biomass. Journal of Environmental Chemical Engineering, 10(2), 107200. https://doi.org/10.1016/j.jece.2022.107200

Mishra, S., Sahu, J. N., & Patel, R. K. (2022). Role of organic matter in Cr(VI) reduction. Sustainable Environment Research, 32, 1–10. https://doi.org/10.1186/s42834-022-00131-5

Moggridge, G. D., et al. (2020). Precipitation and removal mechanisms of copper ions in alkaline media. Chemical Engineering Transactions, 82, 499–504. https://doi.org/10.3303/CET2082084

Mohan, D., & Pittman, C. U., Jr. (2006). Activated carbons and low-cost adsorbents for heavy metal removal. Journal of Hazardous Materials, 137(2), 762–811. https://doi.org/10.1016/j.jhazmat.2006.03.060

Mortada, W. I., et al. (2023). H_2O_2-driven degradation of organics in industrial effluents. Process Safety and Environmental Protection, 175, 315–327. https://doi.org/10.1016/j.psep.2023.05.020

Mustapha, S., et al. (2020). Overview of tannery wastewater characteristics and treatment methods. Applied Water Science, 10, 199. https://doi.org/10.1007/s13201-020-01231-4

Omor, J., et al. (2021). Sedimentation and pretreatment of high-strength industrial wastewater. Water Practice and Technology, 16(3), 843–852. https://doi.org/10.2166/wpt.2021.048

Politi, M., & Sidiras, D. (2020). Preparation and characterization of lignocellulosic sorbents. Bioresource Technology Reports, 11, 100516. https://doi.org/10.1016/j.biteb.2020.100516

Rakhunde, R., Deshpande, L., & Juneja, H. (2012). Sulfate concentration in industrial effluents. International Journal of Research in Engineering and Technology, 1(6), 84–88.

Rao, P. V., et al. (2020). Competitive adsorption of heavy metals using agricultural waste. Water Practice and Technology, 15(1), 1–12. https://doi.org/10.2166/wpt.2020.003

Saha, B., & Sanyal, S. K. (2010). Precipitation behaviour of zinc in alkaline solutions. Journal of Chemical & Engineering Data, 55(7), 2692–2696. https://doi.org/10.1021/je900908p

Sahu, O., Rao, D. G., & Yadav, N. (2023). Treatment strategies for tannery wastewater. Heliyon, 9(2), e13017. https://doi.org/10.1016/j.heliyon.2023.e13017

Suryanto, F., et al. (2024). Settling and solid separation efficiency in high-load wastewaters. Journal of Water Process Engineering, 62, 103134. https://doi.org/10.1016/j.jwpe.2024.103134

Urbina-Suarez, N., et al. (2023). Activated carbon removal of COD from industrial wastewater. Environmental Science and Pollution Research International, 30, 12456–12471. https://doi.org/10.1007/s11356-022-23244-4

Wang, S., et al. (2019). Removal of Cr(VI) using zero-valent iron. Scientific Reports, 9, 40955. https://doi.org/10.1038/s41598-019-40955-6

Webster, T., et al. (2024). Storage stability of wastewater samples for heavy-metal analysis. Water Research, 241, 120173. https://doi.org/10.1016/j.watres.2023.120173

Zewdu, A., & Rao, V. (2022). Iron nanoparticle-functionalized biomass for chromium removal. Bioresource Technology Reports, 17, 100918. https://doi.org/10.1016/j.biteb.2021.100918

Zhang, L., Zhou, Q., & Liu, J. (2021). Selective removal of heavy metals using nanoparticle-modified biosorbents: A review. Journal of Water Process Engineering, 40, 101907. https://doi.org/10.1016/j.jwpe.2021.101907

Zhang, Z., et al. (2021). Assessment of dissolved and suspended solids in industrial wastewaters. Environmental Monitoring and Assessment, 193, 110. https://doi.org/10.1007/s10661-021-08857-9